Fellowship Progress Report 2021-2022

Contents

1. Overview of timeline and progress 1
1.1 Timeline 1
1.2 Progress Update 1
2. Results 2
2.2 Objective 1 | Characterize murine GL261 and CT2A glioma models 2
2.2 Objective 2 | Identifying immune-associated therapeutic vulnerabilities in murine gliomas 3
2.2 Objective 3 | Characterization of GTF-perturbed glioma cells 5
3. Relevant publications 5
4. Financial Statement 6
5. Figures 7

1. Overview of timeline and progress

1.1 Timeline

This report summarizes the project objectives completed in the year 1 and 2 of the fellowship (**Table 1**):

Table 1. Project timeline

Year	0-1	1-2	2-3	3-4
Objective 1	- GBM scRNA-seq - human-mouse GBM comparisons			
Objective 2	- bioinformatic identification of GTFs - *in vitro* CTL-killing CRISPR screen	- *in vitro* validation of GTFs		
Objective 3		- generation of GTF-perturbed GBM cells	- *in vivo* experiments	
Publications				Manuscript prep.

1.2 Progress Update

Data collection for **objectives 1 and 2** is near complete, and the main bioinformatic analyses have been performed (some remaining minor experiments/analyses to establish robustness of findings are underway). Results for these first two objectives are currently being written up into a manuscript that aims to present a comprehensive characterization of the GL261 and CT2A murine gliomas as translational models for human GBM, and provides exciting insights into the similarities and differences between human and murine glioma, effect of *in vivo* microenvironment on GBM heterogeneity, and characterization of the glioma-associated immune along with identification of novel therapeutic targets identified by functional CRISPR-based genomics. For **objective 3**, transcription factor-perturbed glioma cell lines have been genetically engineered for a selection of transcription factors predicted to govern GBM subtypes (4 transcription

factors; *Prrx1*, *Wwtr1*, *Tcf4*, and *Nfia*). *In vivo* experiments characterizing the effect of transcription factor knockouts are in progress. The results and analyses from objective 3 will be largely completed in year 3 of this fellowship, with the goal of writing up the transcription factor-focused manuscript in year 4.

2. Results

Here I overview updated results/findings from 2021-2022 that pertain to each objective.

2.2 Objective 1 | Characterize murine GL261 and CT2A glioma models

Data collected for Objective 1 during year 1 of this fellowship has now been comprehensively analyzed and the corresponding manuscript is in the process of being drafted. Here I highlight the main findings.

The overarching goal of Objective 1 was to use scRNA-seq to characterize syngeneic murine models, CT2A and GL261, and to compare the biology of these murine models to human GBM to establish the translational potential of murine glioma models.

Summary of results

We first sought to determine how *in vivo* engraftment affects murine glioma models (**Fig 1A**). Comparison of *in vivo* GL261 and CT2A transcriptomes to *in vitro* data showed that *in vivo* GL261 and CT2A cells are significantly less similar than when cultured *in vitro*, suggesting that the *in vivo* microenviroment influences the transcriptomic landscape of glioma cells (**Fig 1B**). Analysis of homogeneity further indicated that glioma cells acquire more transcriptomic heterogeneity in the in vivo setting (**Fig 1C**). These transcriptomic changes were associated with a loss of mesenchymal-like phenotype and acquisition of oligodendrocyte progenitor-like (OPC) and neural progenitor-like (NPC) phenotype in both glioma models (**Fig 1D**). Differential gene expression analysis identified *Tcf4*, a transcription factor predicted to drive developmental-like GBM phenotype (see *Progress Report, Year 1*), as the most upregulated transcript in *in vivo* GL261 and CT2A cells, whereas *Vim*, a mesenchymal marker, was the top downregulated transcript *in vivo* (**Fig 1E, F**). These findings were corroborated by additional pathway analyses (**Fig 1G, H**), verifying that *in vivo* engraftment of tumors is associated with an acquisition of a NPC/OPC-like phenotype, and loss of mesenchymal-like phenotype in GL261 and CT2A cells.

Having discerned the differences between *in vitro* and *in vivo* glioma cells, we next focused on characterizing *in vivo* GL261 and CT2A cells (**Fig 2A**). We first evaluated whether GL261 and CT2A resemble low- or high-grade human gliomas. Using public scRNA-seq data from WHO grade II and IV human gliomas profiled by Yu et al. (2018) and Abdelfattah et al. (2021), we demonstrated that both murine syngeneic models resemble grade IV glioblastomas better than grade II gliomas (**Fig 2B**, *top and middle panels*). Furthermore, both murine models were more similar to primary GBMs, than recurrent GBMs (**Fig 2B**, *bottom panel*). We next characterized the intrinsic biological pathways that are active in GL261 and CT2A glioma cells using unsupervised NMF gene program discovery (**Fig 2C-E**). Eight gene programs (G1-G8) were identified between the two glioma models. GL261 preferentially expressed a GL261-specific program (G8) along with an OPC-associated (G7) and inflammatory program (G5). In contrast, CT2A cells preferentially expressed three distinct mesenchymal-like programs (G4; MES1, G6; MES2, and G2; MES3), along with a CT2A-specific program (G3). Both glioma lines expressed a cell cycle-associated program (G5). Importantly, the gene programs observed in GL261 and CT2A cells are reminiscent of gene programs observed in human GBM, including developmental-like states (OPC, NPC and AC subtypes) and mesenchymal-like states (MES subtypes) (Neftel et al. 2019, Richards et al. 2021). We finally evaluate the prognostic value of these gene programs, and while they did not predict survival among GBM patients, these gene programs were strongly prognostic among low-grade gliomas (**Fig 2F**). Specifically, GL261-

specific and OPC-like program activity was associated with better prognosis, whereas inflammatory, cell-cycle, and MES1 program activity was associated with poor prognosis.

In establishing GL261 and CT2A as relevant translational models of GBM, we also compared the genetic dependencies of murine GBM to human GBM (**Fig 3A**). We performed a pooled loss-of-function genetic screen across CT2A and GL261 cell lines and identified essential fitness genes using BAGEL (**Fig 3B;** BF > 5 threshold). We then compared these to essential fitness genes identified across 41 human GBM lines (*Project Score*) and found that CT2A cells recapitulate human essential fitness genes with an AUROC of 0.91, and GBM-specific essential genes with an AUROC of 0.71 (**Fig 3C**). Analysis of enrichment maps derived from CT2A and human GBM-specific genetic dependencies revealed that CT2A recapitulate common and GBM-specific genetic dependencies associated with RNA processing, epigenetic regulation, and cell cycle (**Fig 3D**). The genetic dependencies that were unique to human GBM (i.e., not observed in CT2A cells) were proteoglycan biosynthesis, protein UFMylation, and cell polarity/migration-associated processes. Together these analyses suggest that the GBM-related biology observed CT2A and GL261 murine models is relevant to human GBM and identifies GBM-specific biology that is not recapitulated by murine models.

Next steps

Analysis of GL261 genetic screen results are still in progress, and will eventually replace the placeholder panels in **Fig 3B**, **C** and **E**. Once a few additional (minor) experiments/analyses intended to ensure the robustness of findings are complete, results from this objective will be written up into a manuscript that provides a comprehensive characterization of GL261 and CT2A as translational murine models of GBM.

2.2 Objective 2 | Identifying immune-associated therapeutic vulnerabilities in murine gliomas

Objective 2 is concerned with identifying GBM-subtype-specific transcription factors (GTFs). I had originally proposed to identify GTFs using two independent and complementary strategies, the first involving a bioinformatic analysis of transcription factor activities in GBM (results summarized in *Progress Report, Year 1*) and the second involving an *in vitro* genome-wide CRISPR screen using cytotoxic T-lymphocyte (CTL) and murine glioma cell co-cultures to identify genes that confer cancer immune evasion, and represent potential targets for immunotherapy. In the current progress report, I summarize findings from the latter strategy, that focuses on immune-tumor interactions.

Summary of results

The *in vivo* glioma-associated immune microenvironment was first characterized using scRNA-seq profiles of sham, GL261- and CT2A-engrafted brain samples (**Fig 4A, B**). We identified 4 major immune cell populations, representing macrophages (Mp), microglia (Mg), dendritic cells (D) and T cells (T), that were further stratified into 14 subpopulations (**Fig 4B**). Macrophages (Pid1+/Zeb2+) represented the most diverse and abundant population, comprised of 7 subpopulations, and were characterized by gene programs implicated in TNFα signaling (Lyn+ Mp-4 cells), Hypoxia (Abca1+ Mp-5 cells), IFN signaling (Cxcl10+ Mp-9 cells), antigen presentation (Mp-8, Mp-9, Mp-14 cells), and cell cycling (Negr1+ Mp-8 cells). T-cells (Skap1+/Tox+) consisted of 3 subpopulations, including Ctla4+ T-regulatory cells (T-11), and dendritic cells consisted of 2 subpopulations, including a Cd74+ subset (D-12) and Stat4+ subset (D-15). Finally, the microglial population consisted of 2 subpopulations, with the smaller Mg-3 subset representing an intermediary phenotype between microglial Mg-2 cells and the surrounding Slc9a9+ macrophage population (Mp-14). We also considered the extent to which the murine immune microenvironment recapitulates human GBM (**Fig 4C**; **Fig S2**). Comparing immune-intrinsic immune programs derived from

murine glioma models (GL261 and CT2A) and human GBM samples (Neftel, Abdelfattah and Yu GBM cohorts), we found that the major gene programs, including cell cycle, T-cell differentiation, hypoxia, IFN signaling, and TNFα signaling were consistently observed (**Fig 4C**). MHC class I antigen presentation and lipid metabolism were the only human-derived programs that were no recapitulated in either murine model. Taken together, we conclude that the CT2A and GL261 immune microenvironments represent approximate models of the immune microenvironment observed in the setting of human GBM.

We next performed a compositional analysis to identify the major immune populations that are recruited upon glioma engraftment, and to determine whether there are any differences in immune cell composition between the GL261 and CT2A models. In sham control mice, immune cells represented 1.1% of the total sample profiled by scRNA-seq, compared to 5.3% and 2.1% in CT2A and GL261 cells, respectively (**Fig 4D**). Notably, GL261 and CT2A engraftment was associated with significant recruitment/activation/ expansion of the IFN-signaling macrophages (Mp-9), CTLA+ T-regulatory cells (T-11), activated and cycling T cells (T-6), antigen-presenting dendritic cells (D-12 and D-15), and microglial cells (Mg-2) (**Fig 4E**). Differential abundance analysis further revealed that TNFα signaling macrophages (Mp-4) and cycling macrophages (Mp-8) was preferentially enriched in CT2A whereas the Mp-3 microglial population was enriched in GL261 cells (**Fig 4F**).

Having characterize the immune microenvironment in CT2A and GL261, we sought to focus on the interactions between T cells and glioma cells to identify putative immunotherapy targets. We performed a pooled loss-of-function genetic screen using CT2A cells expressing ovalbumin (Ova) as marker antigen. CRISPR-mutagenized cells were propagated in the present or absence of preactivated antigen-specific CTLs to apply a selection pressure, with representative cell populations serially sampled at days 0 and 19 and subjected to deep sequencing to identify gRNAs that were enriched or depleted relative to untreated cell populations. To identify genes involved in cancer-intrinsic CTL evasion, differential fitness effects in CTL-treated versus control population were quantified using the drugZ algorithm (10% FDR) (**Fig 4G**). Among the suppressors (i.e., gene perturbations that confer resistance to CTL killing) were IFNγ/JAK/STAT signaling genes (*Jak2*, *Jak1*, *Ifngr2*, *Stat1*) and chromatin remodeling-associated genes, whereas sensitizers (i.e., gene perturbation that confer sensitivity to CTL killing) were related to macroautophagy (*Atg3*, *Atg12*, *Atg9a*, *Atg101*) and TNFα signaling (*Traf2*) (**Fig 4H**). We did not identify any GTFs in this CRISPR screen. Nonetheless, we further pursued *Atg12*, a gene involved in the macroautophagy pathway. Atg12 perturbed CT2A and GL261 lines (*ΔAtg12*) were generated (**Fig S3**) and CT2A cells were engrafted into mice to evaluate effect of macroautophagy disruption on survival (**Fig 4I**). Consistent with prediction from the *in vitro* CTL-evasion screen, we found that *ΔAtg12* CT2A-engafted mice had prolonged survival, compared to parental controls. These results suggest that macroautophagy places a critical role in CTL-mediated killing of glioma cells, and that disruption of *Atg12* may represent a feasible target for targeted immunotherapies.

Next steps

In vivo experiments evaluating the survival of mice engrafted with the *ΔAtg12* GL261 cell line are currently underway and are intended to complement results from CT2A cells. Since no GTFs were identified in the CTL-kill screen, no additional hits from this experiment will be pursued in Objective 3. However, given the observation that GL261 and CT2A are associated with differential cytokine profiles (IFNγ signaling in GL261 tumors, and TNFα in CT2A), I hypothesize that the two glioma models may have differential sensitivities to IFNγ and TNFα, which represents an important consideration when selecting glioma models for immunotherapy-related research. Experiments evaluating the differential sensitivity of GL261 and CT2A cells to IFNγ and TNFα and will be included in the first manuscript that characterizes GL261 and CT2A as translational murine models of GBM.

2.2 Objective 3 | Characterization of GTF-perturbed glioma cells

Summary of results

Objective 3 aims to characterize GTF-perturbed glioma cell lines. I previously identified candidate GTFs through bioinformatic analysis of a collection of public and in house scRNA-seq GBM data (these analyses are summarized in *Progress Report, Year 1*). From these analyses, I selected 4 candidate GTFs, 2 predicted to govern the mesenchymal-like phenotype in GBM (*Wwtr1* and *Prrx1*), and 2 predicted to govern the developmental-like phenotype in GBM, and generated CRISPR-Cas9 edited cell lines harboring loss-of-function perturbation for each candidate GTF (**Fig 5**).

Next steps

In vivo experiments characterizing GTF-perturbed CT2A cells are currently underway. Following engraftment of individual GTF-perturbed CT2A cells, murine survival will be assessed, and tumor samples will be obtained at end-point for downstream scRNA-seq characterization. GL261-perturbed cell lines are also in the process of being generated, to provide complement results in CT2A cells.

3. Relevant publications

In addition to the funded project, I have actively participated and contributed to several GBM-related collaborations, amounting to 4 publications that have been accepted/published (4 co-author), and an additional 5 publications in review/revision (2 first-author, 3 co-author).

Accepted/Published

1. Han H.*, Best AJ.*, Braunschweig U.*, **Mikolajewicz N.**, Li J., Roth., Chowdhury F., Mantica F., Nabeel-Shah S., Parada G., Brown K., O'Hanlon D., Wei J., Yao Y., Abou Zid A., Comsa E., Jen M., Wang J., Datti A., Gonatopoulos-Pournatzis T., Weatheritt RJ., Greenblatt JF., Wrana JL, Irimia M., Gingras A, Moffat J., Blencowe BJ. (2022). Systemic exploration of dynamic splicing networks reveals conserved multistage regulators of neurogenesis. *Mol Cell.* doi: 10.1016/j.molcel.2022.06.036. *contributed equally.
2. Seyfrid M., Maich WT., Shaikh VM., Tatari N., Upreti D., Piyasena D., Subapanditha M., Savage N., McKenna D., **Mikolajewicz N**., Han H., Chokshi C., Kuhlmann L., Khoo A., Salim SK., Archibong-Bassey B., Gwynne W., Brown KR., Murtaza N., Bakhshinyan D, Vora P., Venugopal C., Moffat., Kislinger T., Singh SK. (2021). CD70 as an actionable immunotherapeutic target in recurrent glioblastoma and its microenvironment. *J Immunother Cancer.* 10(1):e003289. doi: 10.1136/jitc-2021-003289.
3. Qazi M., Salim SK., Brown KR., **Mikolajewicz N**., Savage N., Hong H., Subapanditha MK., Bakhshinyan D., Nixon A., Vora P., Desmond K., Chokshi C., Singh M., Khoo A., Macklin A., Khan S., Tatari N., Winegarden N., Richards L., Pugh T., Bock N., Mansouri A., Venugopal C., Kislinger T., Goyal S., Moffat J., Singh SK. (2022). Characterization of the minimal residual disease state reveals distinct evolutionary trajectories of human glioblastoma. *Accepted (Cell Reports).* doi: 10.1101/2022.01.28.478232
4. Tang Y., Qazi MA., Brown KR., **Mikolajewicz N**., Moffat J., Singh SK., McNicholas PD. (2021). Identification of five important genes to predict glioblastoma subtypes. *Neuroncol Adv.* 3(1):vdab144. doi: 10.1093/noajnl/vdab144

In review or revision / Preprint

1. **Mikolajewicz N**., Brown KR., Moffat J., Hong H. (2022). Multi-level cellular and functional annotation of single-cell transcriptomes. *BioRxiv* and *in revision* (*Communication Biology*).

2. **Mikolajewicz N**., Khan S., Trifoi M., Skakdoub A., Ignatchenko V., Mansouri S., Zuccatto J., Zacharia BE., Glantz M., Zadeh G., Moffat J., Kislinger T., Mansouri A. (2022) Leveraging the CSF proteome toward minimally-invasive diagnostics and biological characterization of brain malignancies. *Medrxiv* and *in revision (Neuro-Oncology Advances*).
3. Gwynne WD., Suk Y., Custers S., **Mikolajewicz N**., Chan JK., Zador Z., Zaslaver O., Bakhshinyan D., Chokshi C., Burns I., Chaudhry I., Nachmani O., Mero P., Brown K., Quaile AT., Venugopal C., Moffat J., Montenegro-Burke JR., Singh SK. (2022). Cancer-selective metabolic vulnerabilities in MYC-amplified medulloblastoma. *In revision* (*Cancer Cell*).

4. Tatari N., Khan S., Livingstone J., Mckenna D., Ignatchenko V., Chokshi C., Gwynne WD., Singh M., Revill S., **Mikolajewicz N**., Zhu C., Chan J., Hawkins C., Lu JQ., Provias JP., Ask K., Morrissy S., Brown S., Weiss T., Weller M., Greenspoon JN., Moffat J., Venugopal C., Boutros PC., Singh S., Kislinger T. (2022) The proteomic landscape of glioblastoma recurrence reveals novel and targetable immunoregulatory drivers. *In review.*

5. Zuccato JA., Patil V., Mansouri S., Voisin MR., Chakravarthy A., Shen SY., Nassiri F., **Mikolajewicz N**., Trifoi M., Skakdoub S., Zacharia BE., Glantz M., De Carvalho DD., Mansouri A., Zadeh G. (2022) Diagnostic utility of cerebrospinal fluid methylome-based liquid biopsies for malignant brain neoplasms. *In review*.

4. Financial Statement

Table 2. Financial Expense Report

Term	**Description**	**Amount ($)**
2020-2021	Salary support	20625.00
2020-2021	Conference Registration	25.85
2020-2021	Bioinformatics Computer	3460.81
2021-2022	Salary support	22500.00
	Total	**46611.66**

5. Figures

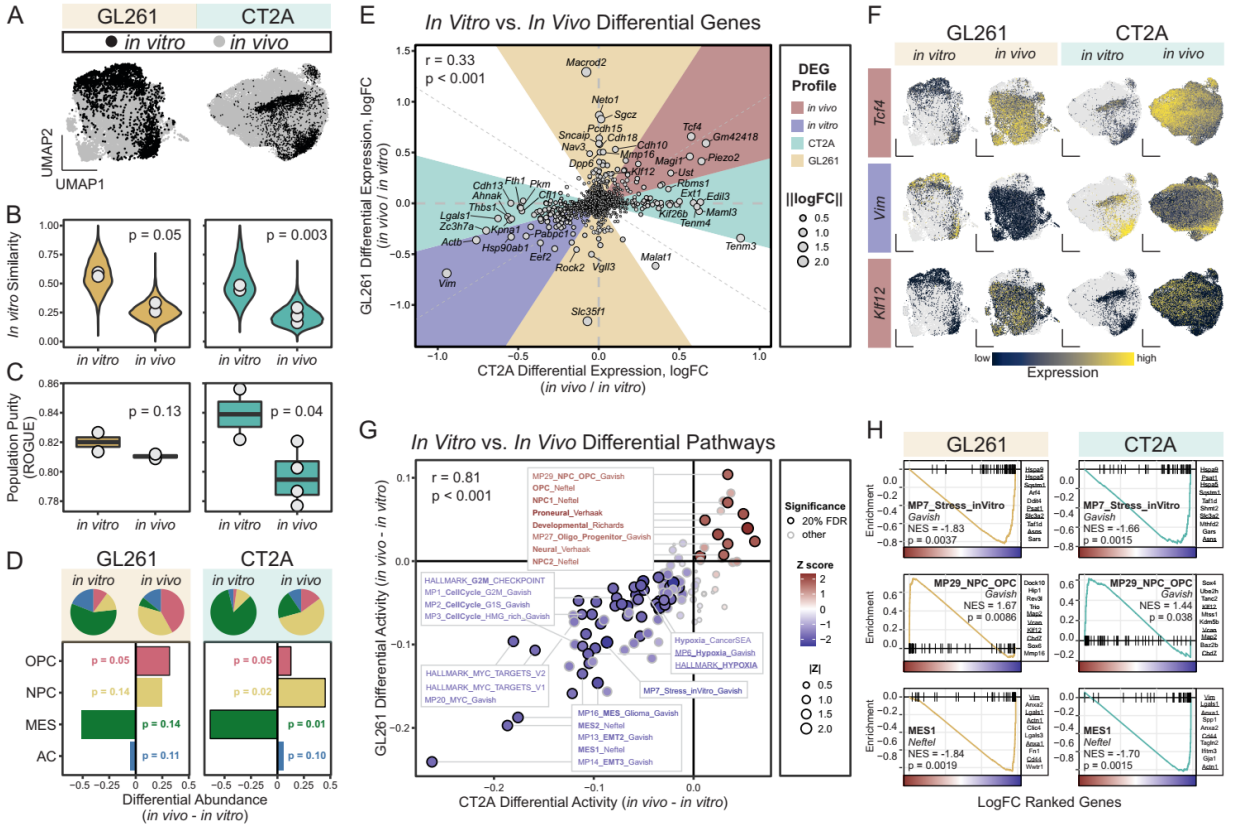

Figure 1. *in vitro* vs. *in vivo* comparison of syngeneic glioma models. **(A)** UMAPs of *in vitro* and *in vivo* GL261 (*left panel*) and CT2A (*right panel*) glioma cells. **(B)** Similarity of *in vitro* and *in vivo* single cell transcriptomic profiles to pseudobulk *in vitro* references quantified by correlation coefficient (R^2). *In vitro* vs. *in vivo* similarities compared by Wilcoxon test. **(C)** *In vitro* vs. *in vivo* population purity (i.e., homogeneity), quantified by ROGUE and compared by Wilcoxon test. **(D)** Abundance analysis of GBM subtype (Neftel 2019) *in vitro* vs. *in vivo*. *Top panel* shows relative abundances in pie charts, and *bottom panel* shows differential abundances (*in vitro* vs. *in vivo*) in bar chart. **(E-F)** Differential gene expression between *in vitro* and *in vivo* GL261 and CT2A glioma cells. Log fold changes (logFCs) are compared between cell lines in sectored scatter plot (**E**) and representative expression profiles are shown as UMAPs (**F**). **(G-H)** Differential pathway activities between in vitro and in vivo GL261 and CT2A glioma cell. Differential activities are compared between cell lines in scatter plot (**G**) and representative GSEA plots are shown (**H**). AC, astrocyte-like; GSEA, gene set enrichment analysis; MES, mesenchymal-like; NPC, neural progenitor-like; OPC, oligodendrocyte progenitor-like.

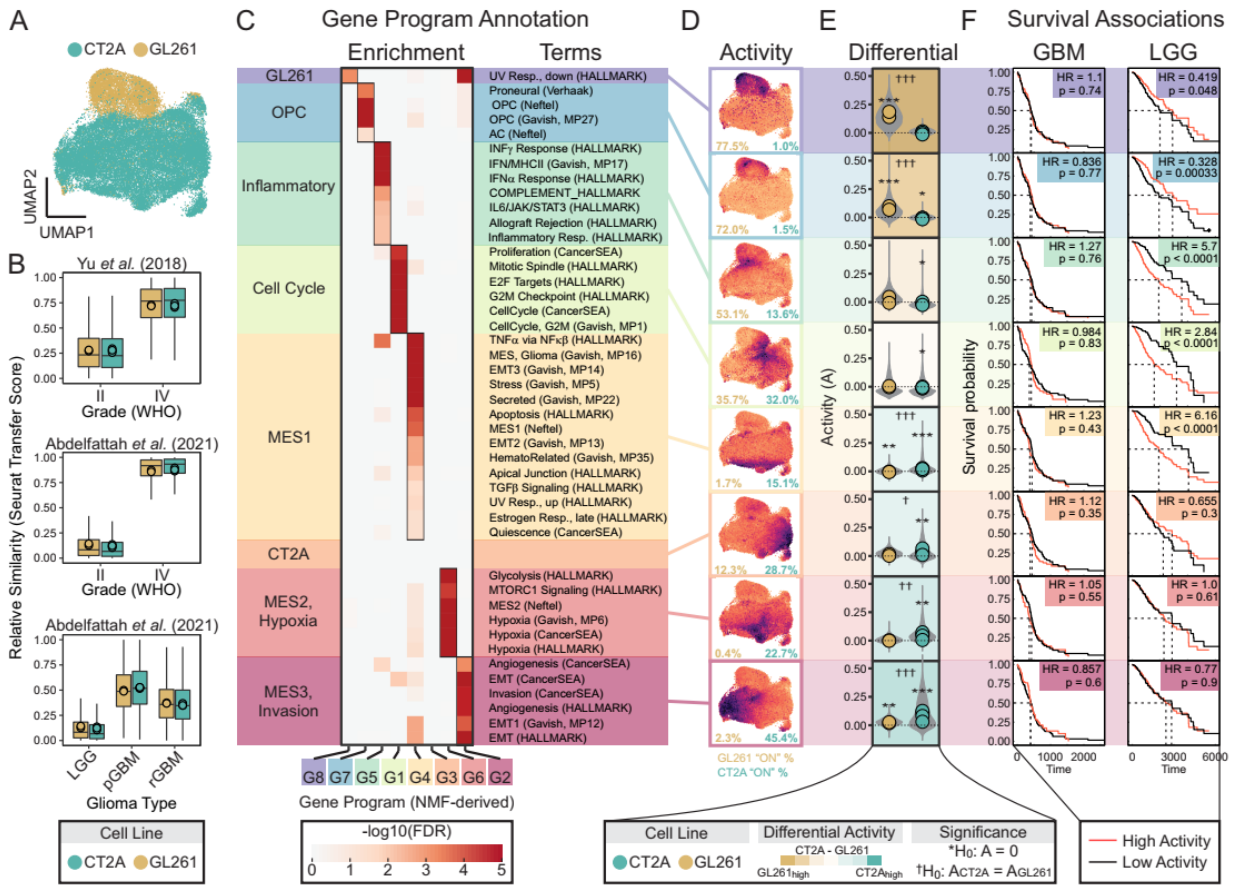

Figure 2. *in vivo* characterization of GL261 and CT2A tumor biology. **(A)** UMAPs of *in vivo* GL261 and CT2A glioma cells. **(B)** Similarity of GL261 and CT2A glioma cells to human WHO Grade II and IV glioma cells (*top and middle panels*), and primary vs. recurrent GBM (*bottom panel*). Relative similarities estimated using Seurat Transfer Score algorithm. **(C-F)** GL261- and CT2A-intrinsic gene programs were discovered using unsupervised NMF algorithm and characterized using hypergeometric gene set enrichment (**C**), gene program activity visualization on UMAPs (**D**), differential gene program activity between CT2A and GL261 glioma cells (**E**), and survival analysis using LGG and GBM patient data from TCGA (**F**). GBM, glioblastoma; LGG, low grade glioma.

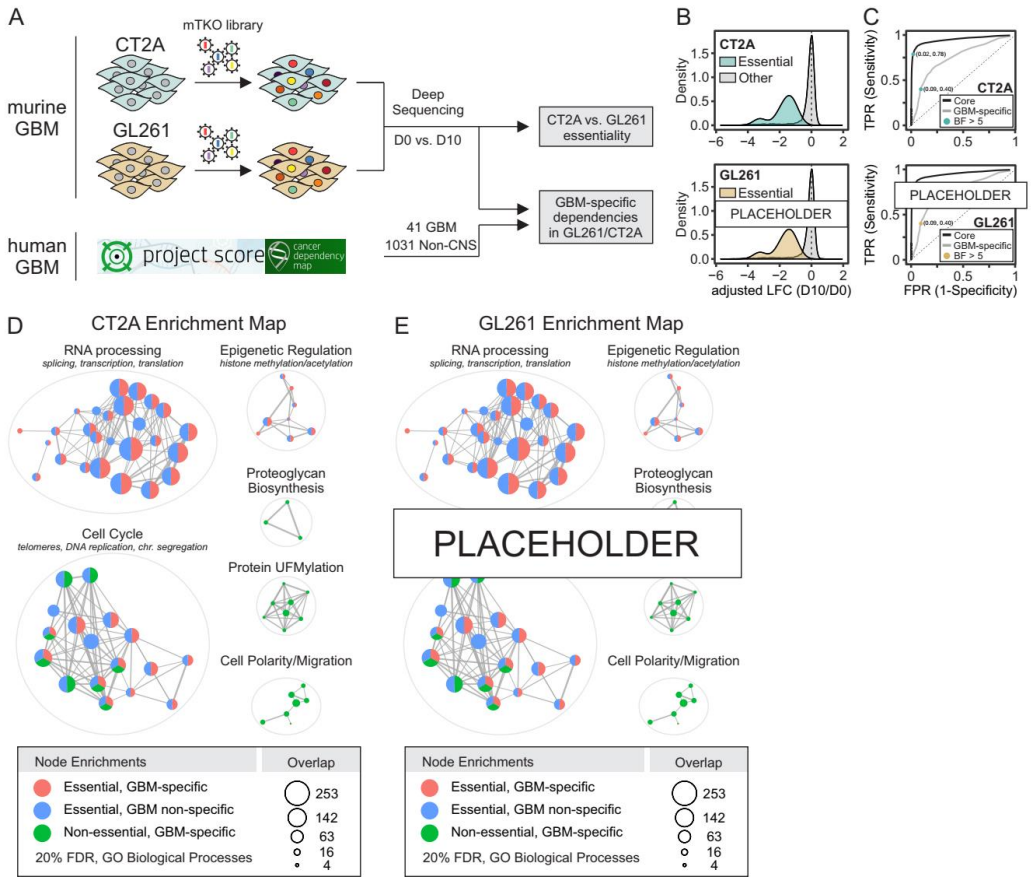

Figure 3. Genetic dependencies in murine and human glioblastoma. **(A)** Workflow for mTKO genome-scale pooled CRISPR screens to identify fitness genes in CT2A and GL261 cells. Core and GBM-specific fitness genes in human GBM were obtained using 41 GBM lines and 1031 Non-CNS lines. **(B)** Distribution of gene-level differential logFC of gRNAs in CT2A (*top*) and GL261 (*bottom*), stratified by essentiality. Essential genes were identified using BAGEL, with BF > 5 threshold. **(C)** ROC analysis of core and GBM-specific fitness gene recovered using CT2A (*top*) and GL261 (*bottom*) CRISPR screens. Human GBM fitness genes were used as ground-truths. **(D-E)** Enrichment map showing fitness-associated pathways in CT2A (*left*) and GL261 (*right*). Genes that were essential in human GBM, but not murine models, were also included to identify differential genetic dependencies between human and murine GBM. Note that bottom panels of C and D, and E are placeholders for GL261-specific data (*analysis in progress*).

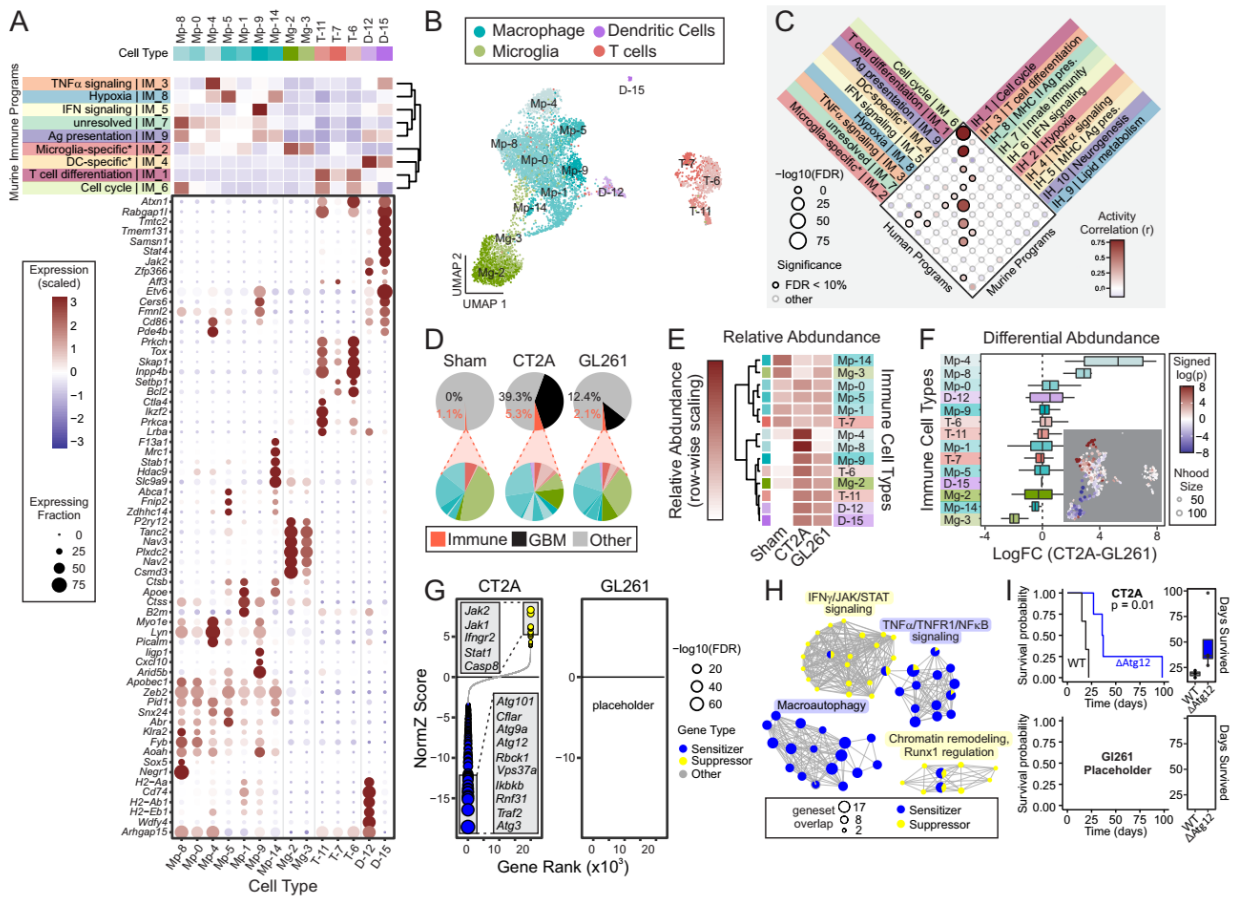

Figure 4. Immune microenvironment in glioma-engrafted murine brains. **(A)** Gene program activity (*top heatmap*) and marker gene expression (*bottom dot plot*) in immune cells types. **(B)** UMAP of immune cells recovered from sham, GL261, and CT2A-engrafted brains. **(C)** Comparison of murine and human immune-associated gene programs. *Size and outline of dots* reflect degree of enrichment of murine gene sets in human gene sets, and *color of dots* reflects correlation between murine and human gene program activities scored in murine immune population. **(D-E)** Relative abundance of immune populations in samples obtained from sham, GL261, and CT2A-engrafted brains represented using pie chart (**D**) and heatmap (**E**). Relative abundances in heatmap (**E**) have been scaled row-wise to facilitate cell type comparison between experimental conditions. **(F)** Differential abundance analysis of CT2A vs. GL261 immune populations using Milo algorithm. *Inset*: UMAP of neighborhood-level differential abundance estimates. Each neighborhood is comprised of 50-100 nearest-neighbor cells, and color represents differential abundance between CT2A and GL261 models. *Red and blue color scale*: immune populations enriched in CT2A and GL261 models, respectively. **(G)** Gene-level NormZ scores for genome-wide CRISPR screen in CT2A and GL261 cells propagated in presence or absence of CTL cells. Hits at 5% FDR are highlighted in *yellow* (resistor genes) and *blue* (sensitizer genes), and top genes are indicated for each category. *Dot size* is inversely scaled by FDR. **(H)** Enrichment map showing CTL resistance (*yellow*) and sensitization (*blue*) pathways enriched in CT2A cells using hypergeometric gene set enrichment (10% FDR). **(I)** Survival analysis of ΔAtg12 and parental CT2A (*top*) and GL261 (*bottom*)-engrafted mice shown using Kaplan meier curves (*left*) and box plots (*right*). Note that right panel of G, and bottom panel of I are placeholders for GL261-specific data (*analysis in progress*).

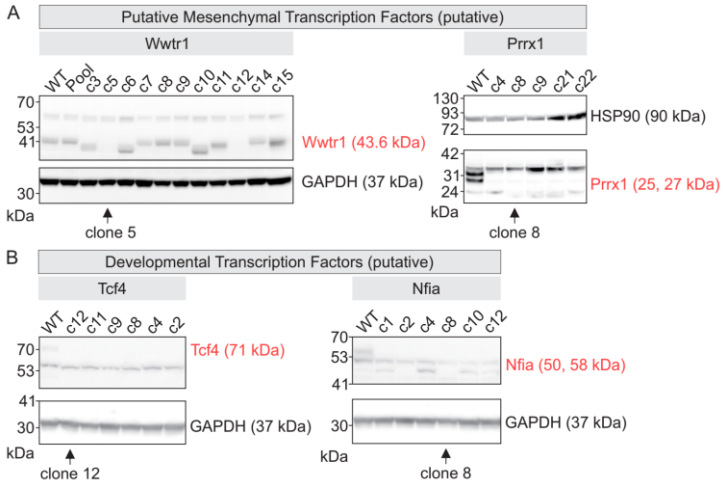

Figure 5. Transcription factor-perturbed CT2A cells. **(A-B)** Immunoblot analyses of transcription factor expression in CRISPR-Cas9-edited CT2A cells. Following CRISPR-Cas9 perturbation, CT2A cells were reseeded at a single-cell density and expanded to generate monoclonal cell lines. Transcription factor (Wwtr1, Prrx1, Tcf4, Nfia) and house-keeping protein (GAPDH or HSP90) expression were assessed by immunoblot analysis in each monoclonal cell line and used to select clonal cell lines for downstream experiments (*indicated by arrow*). Immunoblots for mesenchymal (**A**) and developmental (**B**) transcription factor-perturbed cell lines are shown.

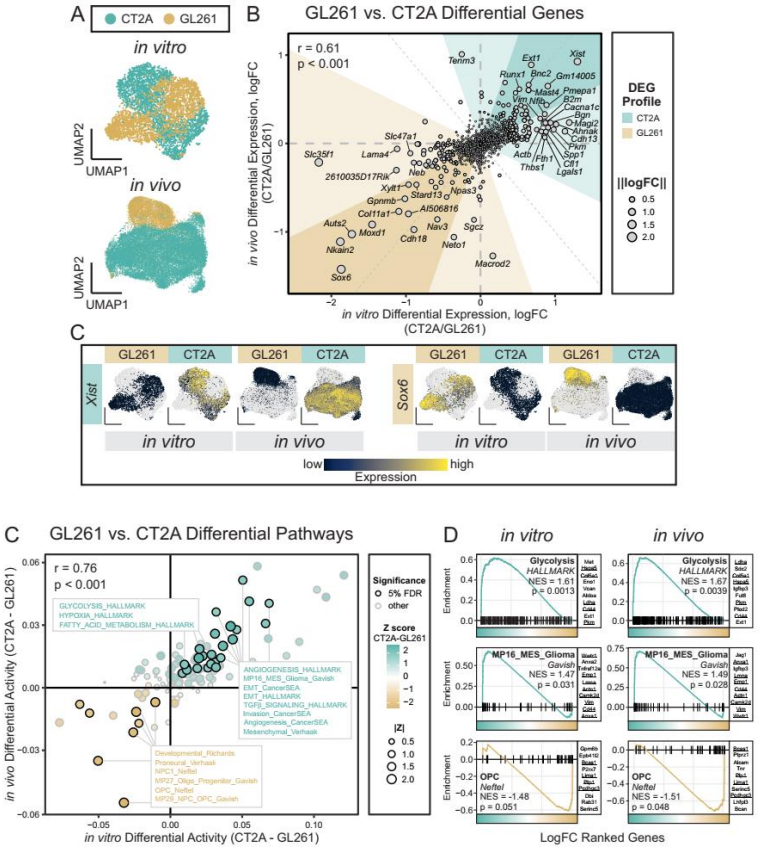

Supplemental Figure 1. Differential gene expression and pathway activities between CT2A and GL261 cells (A) UMAPs of CT2A and GL261 *in vitro* (*top*) and *in vivo* (*bottom*). **(B)** Sectored scatter plot summarizing differential gene expression between GL261 and CT2A glioma cells *in vitro* (*x-axis*) and *in vivo* (*y-axis*). (**C)** Representative marker genes shown on UMAP. **(D-E)** Differential pathway activities between GL261 and CT2A glioma cells *in vitro* (*x-axis*) and *in vivo (y-axis)*. Differential activities are compared between cell lines in scatter plot [**D**; *in vitro* (*x-axis*) and *in vivo* (*y-axis*)] and representative GSEA plots are shown (**E**).

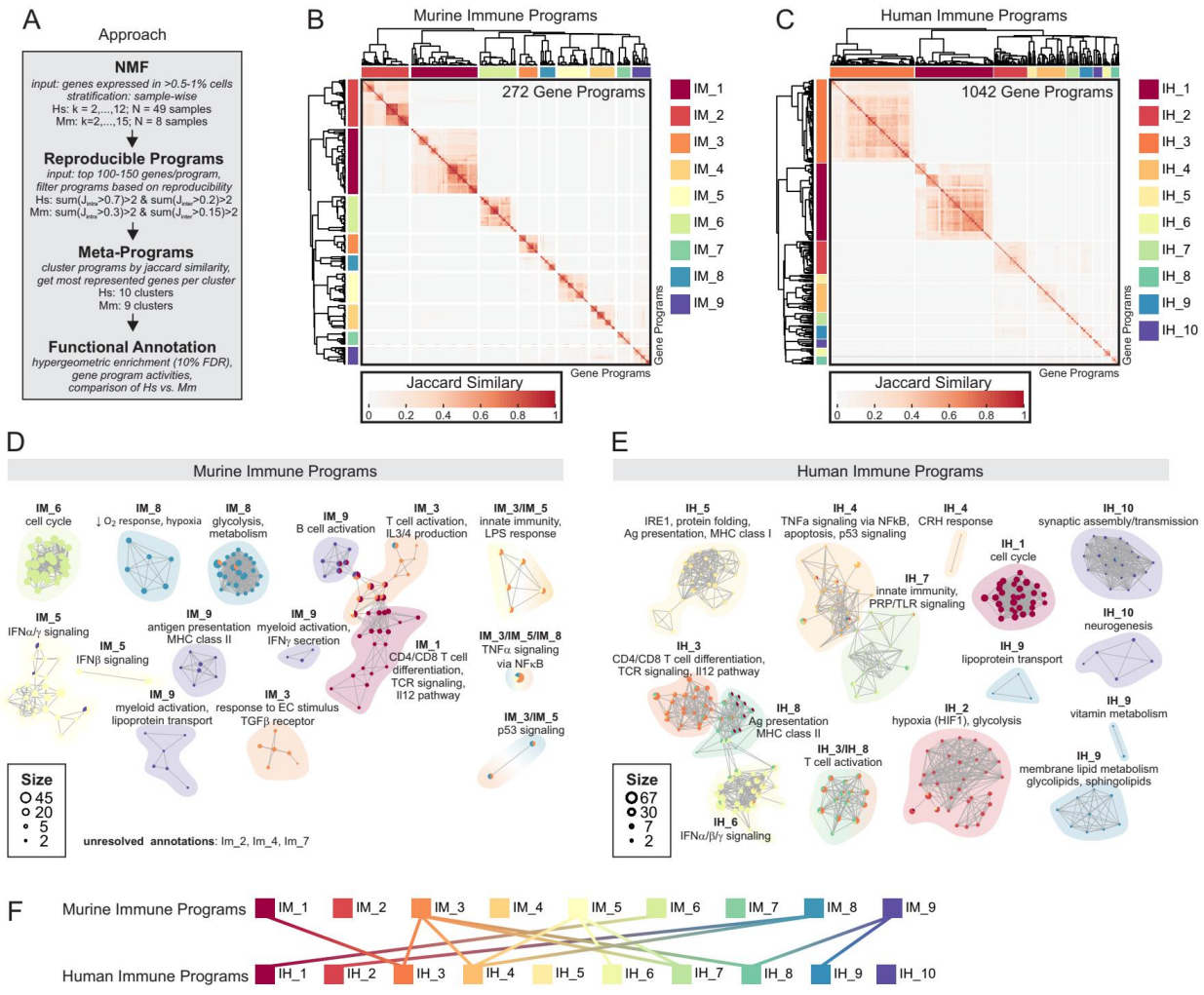

Supplemental Figure 2. Immune-intrinsic gene programs in murine and human GBM. (A) Flowchart for NMF-based gene program discovery and annotation. **(B-C)** Heatmap showing Jaccard similarity indices for comparisons among 272 and 1042 reproducible NMF programs in murine (**B**) and human (**C**) GBM-associated immune populations, respectively, based on top 100-150 genes. Programs were grouped by unsupervised clustering and correspond to immune murine meta-programs (IM) or immune human meta-program (IH). **(D-E)** Enrichment maps showing functional annotations of immune-intrinsic gene programs using hypergeometric gene set enrichment (10% FDR). **(F)** Mapping of murine to human immune programs, based on common term enrichment.

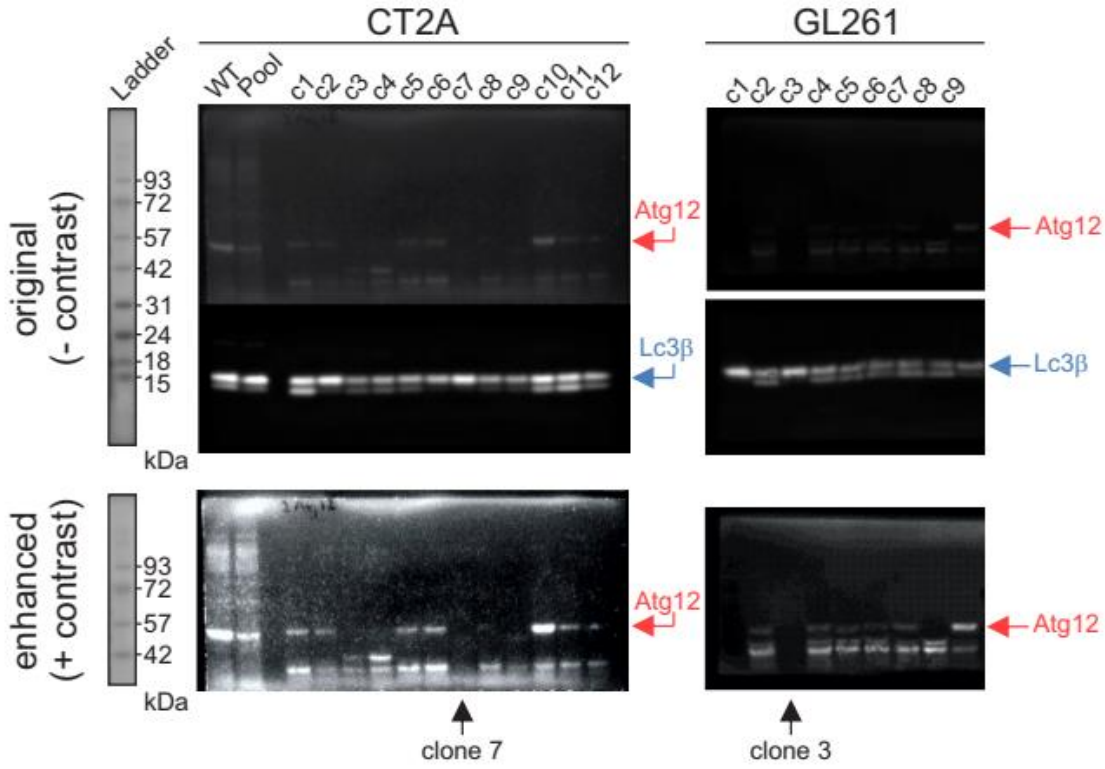

Supplemental Figure 3. Generation of Δ Atg12 CT2A and GL261 cell lines. Immunoblots of candidate Δ Atg12 clones in CT2A (*left*) and GL261 (*right*) cells. *Top panels* are original blots, *bottom panels* are contrast enhanced. Clone 7 (CT2A) and clone 3 (GL261) were selected for downstream experiments. Lc3β expression verifies that other components of autophagy remain intact following CRISPR-mediated perturbation of Atg12.